Russian Geology and Geophysics © 2020, V.S. Sobolev IGM, Siberian Branch of the RAS
Vol. 61, No. 12, pp. 1448–1459, 2020 *DOI:10.15372/RGG2020101* *Geologiya i Geofizika*

Results of Magnetic-Variation Sounding of the Tatar Strait at Two Points on Its Opposite Shores

S.S. Starzhinskii ✉, **V.M. Nikiforov**

V.I. Il'ichev Pacific Oceanological Institute, Far Eastern Branch, Russian Academy of Sciences, 690041, Vladivostok, ul. Baltiiskaya, 43, Russia

Received 22 February 2019; received in revised form 22 January 2020; accepted 31 January 2020

Abstract—Results of magnetic-variation sounding on the opposite shores of the Tatar Strait are presented. The resulting frequency dependences of tippers serve as a basis for 3D inversion carried out using the ModEM software. The inversion yields horizontal and vertical sections of the Tatar Strait in a 400×400×400 km area along the *x*, *y*, and *z* axes, respectively. A conductive zone is revealed near the continental shore, and its central part has an electric resistivity of 0.5 Ohm·m at a depth of 5–7 km. The zone reaches 20–40 km across and vanishes in the lower crust. Along the shore, an anomaly begins north of the Datta Village and extends to the area south of the town of Sovetskaya Gavan. There is a similar anomaly that is isometric in the horizontal plane and less contrasting, which exists near Sakhalin Island at depths of 8–12 km, where the crust resistivity is 15 Ohm·m. The position of the anomaly matches the nearby zone of local $M = 4–6$ earthquakes in the upper crust. At depths greater than 10 km beneath the strait, these anomalies merge and the electrical resistivity increases. In the lower crust and in the upper mantle beneath the strait, the section is characterized by a resistivity of 30–60 Ohm·m. At depths greater than 100 km, there is a conductive layer submerging beneath the Tatar Strait from the Sea of Okhotsk, with conductive branches running from it beneath the Tatar Strait south and north of the Datta Village. The possible causes of near-shore conductive anomalies are discussed.

Keywords: magnetic-variation sounding; 3D inversion; ModEM; geoelectric section; Tatar Strait

INTRODUCTION

Oil and gas fields have been long searched for in the Tatar Strait. For the purpose of studying its geological structure, a large amount of geophysical research has been carried out in the water area of the strait by shipboard seismic, gravimetry, and magnetometry complexes. This results in detailed maps of anomalous gravitational and magnetic fields and seismic sections, illuminating the structure of the Earth's crust. Seismic studies make it possible to dissect the sedimentary strata and determine its configuration, thickness, and foundation relief. On the transverse profiles in the strait, the North Tatar and South Tatar sedimentary troughs are identified. The thickness of the Earth's crust under the Tatar Strait is also estimated (Tronov et al., 1987).

The performed studies made it possible to mainly investigate the structure of the upper part of the Earth's crust of the strait, but, due to their exploration orientation, they did not affect the subcrustal depths. This means that the geological structure of the Tatar Strait should be investigated further, especially its deep section in the lower crust and in the upper mantle in order to determine the position of deep geoelectric inhomogeneities in this area.

The most suitable geophysical research methods for this purpose are seismic tomography along with magnetotelluric (MT) and magnetic-variation (MV) methods. Using MT and MV methods, one can dissect a section by resistivity. Depending on the period of the recorded natural electromagnetic variations, covering the range from 10^{-4} to 10^{4} s, it is possible to investigate the section, starting from the near-surface layers and down to depths of hundreds of kilometers. The rock resistance determined as a result of this investigation depends on the type of rock, its porosity, the nature of the fluid filling the pores, the degree of graphitization of the rock, temperature, etc. With geological interpretation of the results, all this makes it possible to estimate the material composition of anomalous electrically conductive regions in the section and, in some cases, the thermal regime.

When MT and MV methods are used in the water area of the strait, it is necessary to place the recording equipment either on the ice or on the bottom, which is quite possible, but technically difficult to implement at present, although it is the most informative way. Therefore, a decision has been made to record variations on the shores of the Tatar Strait, assuming that it will be possible to study the section under the bottom of the strait in more detail in the future by continuing research on the profiles deeper into the island and the continent and performing data interpretation. This option is also interesting from a different point of view. It is noted

✉ Corresponding author.
E-mail address: ss_stars@poi.dvo.ru (S.S. Starzhinskii)

in (Varnavskii, 1994) that the previously performed geophysical studies do not cover significant areas of near-continental and shallow waters of the strait, to which gravitational and magnetic anomalies gravitate. In this formulation of measurements, the study of the geoelectric section under the bottom of the strait is possible due to the fact that the MV method allows one to estimate the resistivity both under the measurement point and at a distance from it due to the action of the horizontal skin effect in the magnetotelluric field (Berdichevsky and Dmitriev, 2009). This possibility is organically implemented in the method of 3D inversion of MT and MV data, which has been recently developed. Its analysis performed on control digital models is described in (Campanya et al., 2016), confirming its effectiveness. The visualization of the inversion results, carried out with the help of horizontal sections and vertical sections in the color gradation of the resistivity, allows one to outline the abnormal electrical conductivity zones.

Thus, the purpose of this study is to obtain primary information about the geoelectric section and the localization of deep geoelectric inhomogeneities in the Earth's crust and the upper mantle of the Tatar Strait using MV sounding in the applied configuration and using the 3D inversion of experimental data. Moreover, the goal is to consider possible options for the geological interpretation of abnormally conducting zones, taking into account all available geological and geophysical data.

STRUCTURE OF THE TATAR STRAIT ACCORDING TO GEOPHYSICAL DATA

The Tatar Strait separating Sakhalin Island from the mainland stretches in the meridional direction, narrowing to the north and slowly expanding to the south. The depths of the strait slowly increases to the south and from the continent to Sakhalin Island. In the region under study, which covers the southern part of the North Tatar sedimentary trough, they do not exceed 200–300 m with a strait width of about 130 km (https://maps.ngdc.noaa.gov/viewers/bathymetry/). The thickness of the sediments in the Tatar Strait increases eastward and reaches 6–9 km near the shores of Sakhalin Island. The thickness of the Earth's crust under the strait increases in the same direction and reaches maximum values over 30 km under the island. The block of the Earth's crust of the Tatar Strait is separated from the mainland by the Eastern Sikhote-Alin deep fault of subvertical dip. In the coastal part of the continent, there is a mantle ledge near which the thickness of the Earth's crust decreases to 20 km and which extends from Syurkum Cape to the latitude of the city of Sovetskaya Gavan (Esin et al., 1990; Khanchuk, 2004). The Eastern Sikhote-Alin volcanic belt with extensive fissure eruptions of basaltic plateaus in the region under study (the Sovgavan Plateau) stretches along the western side of the strait (Martynov and Khanchuk, 2013). In general terms, the Tatar Strait is a riftogenic asymmetric graben with a thick layer of sediments in the eastern dislocated part and their gentle pinching-out near the western coast of the strait. The asymmetry of the graben is expressed in the greater subsidence of the eastern base of the rift, which appeared during its formation. The seismically active West Sakhalin fault extends along the western coast of Sakhalin Island (Lomtev et al., 2007), separating the island and the Tatar Strait.

The gravitational field of the strait is characterized by low values with extensive local minima of less than –30 mGal, caused by significant thicknesses of sediments within their ranges (Volgin and Senachin, 2006). According to satellite altimetry data, the near-mainland area of the Tatar Strait is distinguished by intense positive isostatic and Bouguer anomalies along its entire length. Similar anomalies are observed near the eastern coast of the strait, except they are less intense there. In the adjacent Sikhote-Alin folded region, there are extensive negative anomalies of the gravitational field, suggesting decompaction in the Earth's crust to depths of 45–60 km (Esin et al., 1992).

In the magnetic field, the Eastern Sikhote-Alin volcanic belt is characterized by intense positive anomalies associated with magma bodies, manifested by basalt-andesite volcanic rocks and intrusions. A detailed examination reveals local bodies with an upper edge at a depth of about 0.5–2.0 km (Volgin and Kochergin, 2006). At a distance from the mainland, the volcanic rocks are replaced by volcanogenic-sedimentary rocks. A similar pattern is observed in the northern part of the strait. Here, the depth to the upper edges of magnetoactive bodies is estimated at 0.5–5.0 km. In the southern part of the strait, weak isometric magnetic anomalies are presented.

The heat flux in the northern and central parts of the Tatar Strait is close to normal values, while the southern part is characterized by anomalous values of about 100 mW/m^2 (Lyubimova et al., 1976; Veselov, 2006).

DATA

In the summer of 2017, magnetic variations were recorded on the continent in the vicinity of Datta Village (DTA, 49.2818° E, 140.3614° N) and on the Sakhalin Island near the Lesogorskoe Village (LSG, 49.4230° E, 142.1190° N) on the coast of the Tatar Strait (Fig. 1). The three components H_x, H_y, and H_z of geomagnetic variations were recorded using a LEMI-025 fluxgate magnetometer (http://www.isr.lviv.ua/lemi025.htm) at point DTA and a similar magnetometer of the LEMI-417M long-period magnetotelluric device (http://www.isr.lviv.ua/lemi417.htm) at point LSG. Variations were recorded in a right-handed coordinate system, with the z axis directed downward and the x axis of the magnetic sensors orientated along the magnetic meridian. At DTA, the recording lasted for 25 days (August 24–Septem-

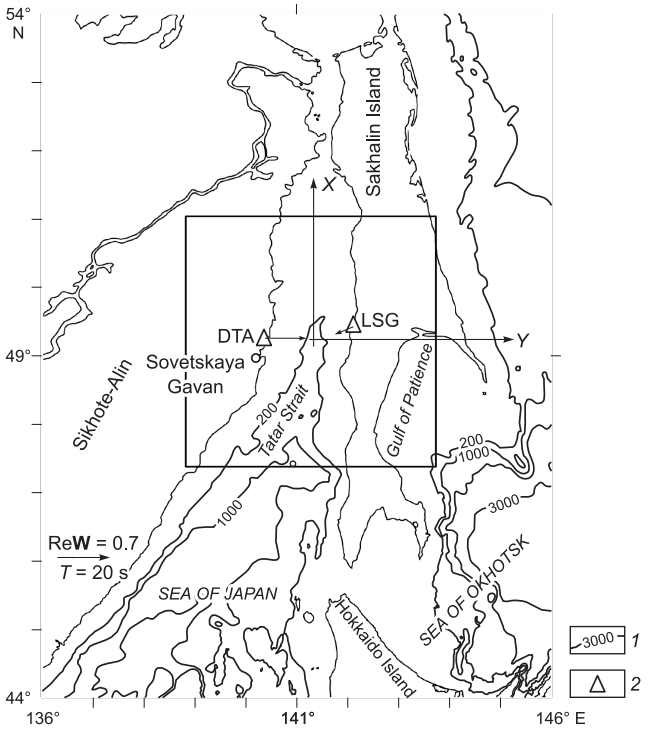

Fig. 1. Location of the central modeling region, the coordinate system, and the real induction arrows on a period of 20 s on the site. *1*, isobaths, m; *2*, observation points: DTA, the Datta Village, LSG, the Lesogorskoe Village.

ber 18, 2017) with a sampling frequency of 1 and 10 Hz. The duration of the observation was determined by the need to record the widest possible range of variation periods and their amplitudes in the short-period region, significantly exceeding the noise. This was especially true considering that the studies were carried out with the minimum solar activity, and it was necessary to record an intense magnetic disturbance.

Fluxgate magnetic field sensors (like those of LEMI magnetic-variation devices) have insufficient sensitivity (high noise level) for recording short-period magnetic variations in a range from 1 to 15 s. This range of variations is recorded by observing the autumnal variation maximum at DTA. The recording time was increased in order to be able to record an intense magnetic storm (September 7–8, 2017, with a daily average index k_p = 49) when the variation amplitude sharply increases, making the signal-to-noise ratio larger. Thus, tippers in this period range are calculated up to a period of 1 s using variations recorded with a sampling rate of 10 Hz.

At LSG, long-term observations were not possible, so the recording lasted from July 3 to July 5, 2017 with a sampling rate of 1 s. At both points, the data were recorded in binary format daily on a flash drive with subsequent conversion into text format by a program included in the equipment set. As the observation results were processes, the data were recalculated into a geographic coordinate system.

PROCESSING OF EXPERIMENTAL DATA

In a frequency domain, between the geomagnetic variation components H_x, H_y, and H_z, the following relationship is fulfilled:

$$H_z = W_x H_x + W_y H_y, \tag{1}$$

Here W_x and W_y are complex values. The complex vector **W**, comprised of W_x and W_y, is written as

$$\mathbf{W} = W_x \mathbf{j} + W_y \mathbf{k}, \tag{2}$$

where **j** and **k** are real directing vectors along the *x* and *y*, respectively, and is called a Wiese-Parkinson vector or A tipper. If Eq. (1) is considered as a scalar product of two complex vectors, namely vector **W** and the vector

$$\mathbf{H}_h = H_x \mathbf{j} + H_y \mathbf{k}, \tag{3}$$

then Eq. (1) can be written as

$$H_z = \mathbf{W}\mathbf{H}_h. \tag{4}$$

Considering the fact that the vector modulus $\mathbf{H}_h$ is expressed as $|\mathbf{H}_h|^2 = \mathbf{H}_h\mathbf{H}_h^*$ and multiplying both parts of Eq. (4) by $(\mathbf{W}\mathbf{H}_h)^*$, in which * denotes a complex conjugation, we obtain

$$|H_z|^2 = |\mathbf{W}|^2 |\mathbf{H}_h|^2. \tag{5}$$

Using Eq. (5), we may express the tipper modulus |**W**| as

$$|\mathbf{W}| = \left(|W_x|^2 + |W_y|^2\right)^{1/2} = \frac{|H_z|}{|\mathbf{H}_h|}. \tag{6}$$

Thus, the tipper modulus denotes the ratio of the vertical variation component modulus to the horizontal component modulus. It is an invariant, i.e., it does not depend on the orientation of the coordinate system. In this case, the tipper phase is determined as

$$\Phi_w = 0.5 \operatorname{arctg} \frac{\operatorname{Im}(W_x^2 + W_y^2)}{\operatorname{Re}(W_x^2 + W_y^2)}. \tag{7}$$

Here Re and Im denote real and imaginary parts of the complex number. For representing the results of MV studies, we introduce a real induction vector Re**W** and an imaginary induction vector Im**W** (induction arrows), determined as

$$\operatorname{Re}\mathbf{W} = -W_{xr}\mathbf{j} - W_{yr}\mathbf{k}, \tag{8}$$

$$\operatorname{Im}\mathbf{W} = -W_{xi}\mathbf{j} - W_{yi}\mathbf{k}. \tag{9}$$

In expressions (8) and (9), in contrast to Wiese's definition, the signs are inverted. In this case, the real induction arrow points to regions of high electrical conductivity. The behavior of an imaginary induction arrow is much more complex and more difficult to simple interpretation. Usually, when the results of MV studies are presented, the values and directions of the arrows are drawn on the maps for a

selected variation period. In this work, the relationship charts of the orientation angles of the real and imaginary arrows on the period (a_r and a_i, respectively). The angles are determined as

$$a_r = \text{arctg}\frac{-W_{yr}}{-W_{xr}} \quad (10)$$

and

$$a_i = \text{arctg}\frac{-W_{yi}}{-W_{xi}} \quad (11)$$

on an interval of 0 – 2π. Positive angles are counted clockwise from north (from the *x* axis). The initial qualitative interpretation is carried out using the tipper modulus and the orientation angles of the induction arrows. The presence of a minimum on the curves showing the dependence of the tipper modulus on the period indicates the presence of a conducting layer in the geoelectric section (Berdichevsky and Dmitriev, 2009), and the orientation of the induction arrows determines the position of a conducting heterogeneity in the horizontal plane relative to a measurement point. We determine which type of geoelectric sections (1D, 2D, or 3D) the section under study belongs to by calculating the tipper skew

$$S_k = 2\frac{W_{xr}W_{yi} - W_{xi}W_{yr}}{|\mathbf{W}|}. \quad (12)$$

In Eq. (12), subscripts *r* and *i* denote the real and imaginary parts of the complex number. The 3D inversion of the interpretation parameters of MV studies is carried out using the values of W_x and W_y at various specified variation periods.

The interpretation parameters defined above are estimated using a specially developed program that includes the following operations: removing a linear trend from the data, correcting the frequency response of channels in the high-frequency domain, performing band-pass filtering in the frequency domain by multiplying the components spectra by the frequency response of a bandpass Gaussian filter, and estimating the functions of multiple, private, and ordinary coherence. Following the inverse Fourier transform of the filtering result in the frequency domain, the envelopes and phases of the narrow-band analytical signal in the time domain are calculated, and coefficients W_x and W_y are calculated at a given time interval sliding over the implementation. The process is finished by robust selection of the calculated coefficients using median estimates and selection for six values of the calculated coherence functions. The maximum length of the input sequences of the program is six days, with a sampling interval dt = 1 sec.

DATA PROCESSING RESULTS

Figure 2 shows the interpretation parameters calculated. Due to the short observation interval, they are determined at a narrower period interval for point LSG than for point DTA. The maximum differences in tipper moduli, shown in the upper part of the figure, are observed in the short- and long-period region, and they have similar values in the intermediate periods. This indicates differences between the upper and lower parts of the geoelectric sections at these points. The real induction vector at point DTA is oriented to the east in latitude, i.e., perpendicular to the coastline. This is indicated by the value of its orientation angle a_r, equal to 90° over the entire range of recorded periods. Given the shallow depths in the Tatar Strait in this region, it can be assumed that, if there are any deep conducting structures, they should be extended parallel to the coast. At point LSG, the orientation of the real induction vector is not so strictly fixed. Here, the orientation angle a_r increases smoothly, reflecting a change in vector directions from west-south-west to west-north-west. In a period range T > 1000 s, there is a sharp change in the direction of the vector; at long periods, this vector is oriented toward the Gulf of Patience in the southeast direction and to the deep-water basin of the Sea of Okhotsk, located at a distance of about 300 km from point LSG. In view of the fact that the depth of the Gulf of Pa-

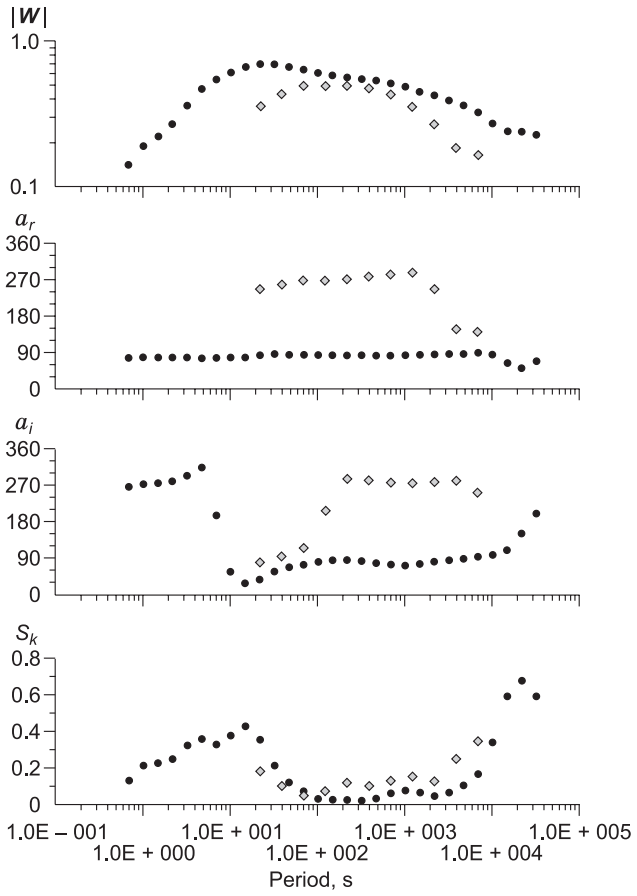

Fig. 2. Charts showing the dependence on the variation period of the calculated tipper modules |W|, azimuths of real a_r and imaginary a_i induction arrows and tipper skew S_k for points DTA (solid circles) and LSG (diamonds).

tience does not exceed 100 m, this orientation of the real vector is determined by the kilometer strata of conductive seawater in the deep-water basin and sedimentary layers of the Gulf of Patience.

The orientation of the imaginary induction vector, characterized by angle α_i, behaves the same way at both points: the imaginary vector is oriented in the direction opposite to the real vector at this point at short periods, and the vectors look in the same direction as the period increases. It is known that, in MV studies, asymmetry S_k characterizes the type of geoelectric section. The section under study is one-dimensional (1D) for $S_k = 0$, it can be considered a two-dimensional (2D) section or close to it for $S_k \le 0.2$–0.3, and this section is three-dimensional (3D) for large S_k. As can be seen from the bottom graph in Fig. 2, the geoelectric section in the vicinity of both points is close to two-dimensional at intermediate periods. Deviations to a three-dimensional section are observed only in the long-period region and at the shortest periods at point DTA.

3D INVERSION

The values of the tipper skew at points DTA and LSG, calculated according to Eq. (12), characterize the section as 2D/3D, and the 3D inversion of tippers may be applied to it. This operation is carried out using a ModEM three-dimensional modeling program with the help of the finite difference method, developed at the University of Oregon, USA (Egbert and Kelbert, 2012; Kelbert et al., 2014). It is successfully applied for the inversion of profile and areal MT and MV experiments (Patro and Egbert, 2008, 2011; Tietze and Ritter, 2013; Kuhn et al., 2014; Samrock et al., 2015; Tietze et al., 2015). ModEM solves a regularized inverse problem by the nonlinear conjugate gradient method, minimizing functional Ψ

$$\Psi(\mathbf{m},\mathbf{d}) = \mathbf{d}-\mathbf{f}(\mathbf{m}))^T \mathbf{C}_d^{-1}(\mathbf{d}-\mathbf{f}(\mathbf{m})) + \lambda(\mathbf{m}-\mathbf{m}_0)^T \mathbf{C}_m^{-1}(\mathbf{m}-\mathbf{m}_0), \quad (13)$$

by minimizing discrepancies in both data and models to obtain an optimal solution to the problem. Here **m** is the matrix of the section model, which optimally satisfies the data matrix **d** and, in this case, the experimental dependences $W_x(f), W_y(f)$, $\mathbf{C}_d = \mathrm{diag}(1/\mathbf{e}_i^2)$, and it is a diagonal matrix containing values inverse to the square of the data errors; **f**(**m**) is the solution matrix of the forward problem for model **m**; $\mathbf{m}_0$ determines the a priori starting model of the section; λ is a regularizing parameter; $\mathbf{C}_m$ is a 3D smoothing and scaling operator. The proximity of the model tippers, obtained at each iteration, to the section tippers obtained experimentally, we calculate the standard deviation (SD) normalized to the error in the data and determined as

$$\mathrm{SD} = \sqrt{\frac{1}{N}\sum_{i=1}^{N}\frac{(d_i^{obs}-d_i^{pred})^2}{e_i^2}}, \quad (14)$$

where d_i^{obs}, d_i^{pred} are the observed and calculated (predicted) tippers for the section model, respectively, and e is the error in the observed tippers. Here the summation is carried out for all measurement points and all periods for which the tippers are calculated. The program is implemented on high-speed multiprocessor systems, which allows calculating complex models of geoelectric sections. The input data of the program can be all components of an impedance matrix or its main elements, tippers, horizontal MV responses, and the main elements of the apparent resistance matrix and its phase, determined on the used period interval. The impedance and tipper values can be fed together to the program input. The role of the starting model of the section can be played by a three-dimensional matrix of resistivity, usually a homogeneous half-space into which a sea or other regions can be included with fixed initial resistivities that change or retain their values during inversion, which is determined by the input data. Smoothing parameters, the initial value of the regularization parameter, the nature of its change in iterations, the maximum number of iterations, and other parameters are also set.

Only tippers are used in the calculations. In this case, there are observations at two points separated by a distance of about 130 km. Therefore, we apply the 3D inversion of the tippers determined at points DTA and LSG. All calculations are performed using the equipment of the Computation Center of the Far Eastern Scientific Center at the Institute of Automation and Control Processes of the Far Eastern Branch of the Russian Academy of Sciences on an IRUS17 multiprocessor computing cluster (https://www.cc.dvo.ru). The grid used is comprised of 86×86×53 cells along the *x*, *y*, and *z* axes, respectively, with no account for the cells in the upper half-space. The *x* axis of the model grid is directed along the meridian northward, the *y* axis eastward, and the *z* axis vertically downward. The origin of the model coordinate system is located in the Tatar Strait at the latitude of point DTA at a node equidistant from both points. Considering the fact that the strait in the region under study is 130-km wide, the *y* coordinates of points DTA and LSG are –65 and 65 km, respectively. Point LSG turns out to be displaced from the *y* axis northward by 15 km along the *x* axis. In the horizontal plane, the central part of a 60×60 grid has a 5×5-km cell, but the cell size increases exponentially toward the edges of the grid with a denominator of 1.24, which determines a modeling area of ≈1095×1095 km. Down the *z* axis, the size of the first cell is set at 50 m and increases with depth in a geometric sequence with a denominator of 1.18. The starting model of the section is set as a half-space with a resistivity ρ = 100 Ohm·m, including the water column of the strait. The resistivity of the water column is set as equal to 0.3 Ohm·m, with it not changing during the counting process. The water column of the strait is approximated by six layers whose horizontal dimensions of which are determined from the bathymetry of the strait, taken from the following website: https://maps.ngdc.noaa.gov/viewers/bathymetry/. Parameters for smoothing the model along the axes are set at

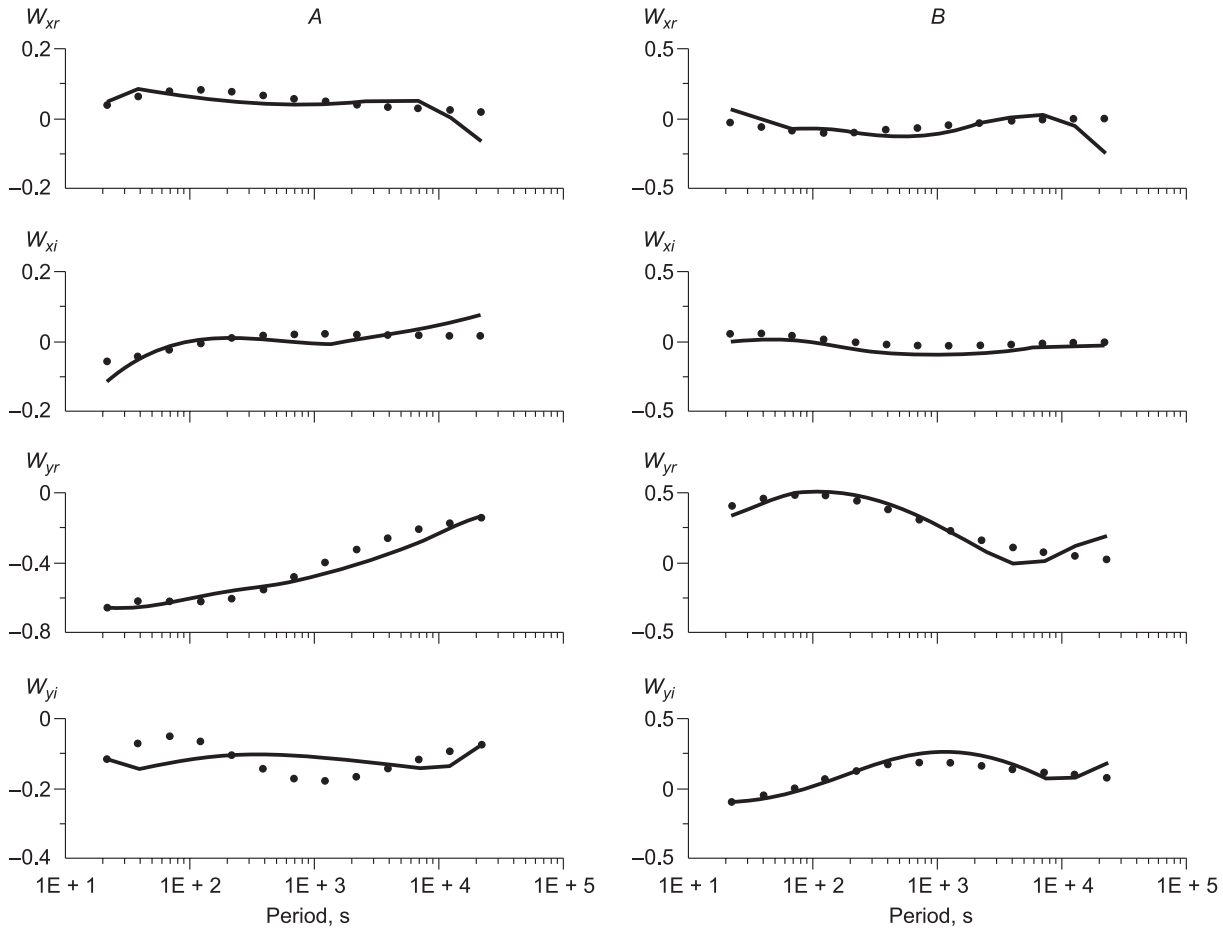

Fig. 3. Real and imaginary parts of experimental tippers (curves) and tippers of the resulting geoelectric section model (solid circles) for DTA (*A*) and LSG (*B*) points.

0.3. The experimental values of the tippers are set for 13 periods, common for both points at an interval of 20–22,000 s. Their error is set to be 0.03 at both points. The proximity of the experimental values of tippers to the predicted values according to the resulting model is estimated according to Eq. (14). Figure 3 shows graphs demonstrating the proximity of experimental and model tippers depending on the variation period for both points with SD = 1.75 after the last iteration.

It should be noted that the above-described inversion is accompanied by 3D inversions based on the data (tippers) of one point of both DTA and LSG to estimate the stability of the inversion results. The models of geoelectric sections in their vicinity are calculated for the following purpose. Some inversions are carried out with a horizontal cell size of 10×10 km in the central part of the modeling region. In addition, some of the starting models have no water layer of the strait, which means that they are set by a homogeneous half-space with ρ = 100 Ohm·m to estimate the effect of conducting seawater on the inversion results. At point DTA, the experimental values of tippers are recalculated into a coordinate system rotated at an angle of 45° to the northwest relative to the original system. In this coordinate system, in which the *x* axis is not parallel to the strike of the strait and the *y* axis is not directed across it, the inversion is carried out. The results of all these inversions indicate that the main features of the section model, obtained in the above-described inversion, are retained in each of them. Differences are observed only in the regions remote from the point when it is inverted according to its data. As the water layer is taken into account, the resistivity of the conductive anomalous zones near the points slightly increases as compared to models that do not take into account the water column.

DATA INVERSION RESULTS

The horizontal slices obtained via inversion and the vertical sections of the resulting model on chosen depths and profiles are illustrated in Figs. 4–6. It should be noted that geoelectric inhomogeneities in the sections are characterized by a wide range of resistivity from 0.5 to 3000 Ohm·m. Of all resulting horizontal slices, Fig. 4 shows the most typical contrasting resistivity distributions in a square area with

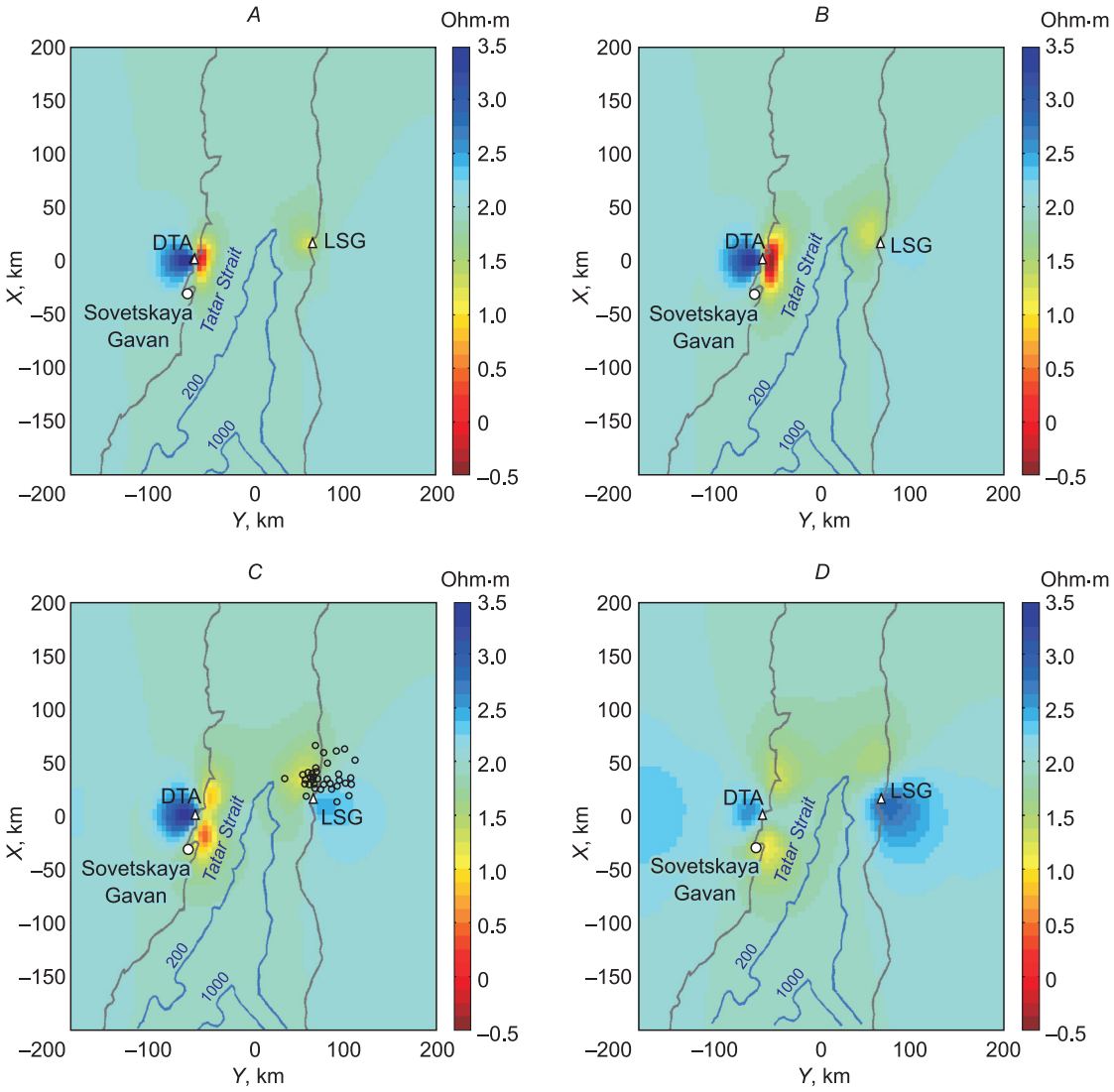

Fig. 4. Resistivity distribution in the resulting model in the *XY* horizontal planes in the modeling regions in layers 3.0–3.6 km (*A*), 6.2–7.3 km (*B*), 10.3–12.2 km (*C*), and 23.9–28.3 km (*D*). Observation points are marked with triangles. On pannel B, the circles show perpendicular projections of earthquake epicenters near point LSG with hypocenters in a depth range from 10 to 12 km, taken from the website http://ds.iris.edu/ieb/index.html, onto the surface of the horizontal section of the model at a depth of 10.3 km. The color scale of the resistivity in a logarithmic scale is shown to the right of the figures. The strait isobaths are given in meters.

a side of 400 km at depths up to 30 km and gradually decaying with increasing depth. As seen from the figure, the inversion results can be used to determine the Earth's crust under the Tatar Strait with the help of lowered resistivity values (30–60 Ohm·m). This suggests that the influence of only the conductive water layer specified in the starting model is insufficient to approximate the experimental frequency dependences of the tippers. Near point DTA, on the side of the strait, one may observe low-resistivity zone parallel to the coastline, which increases in size with depth and reaches a maximum of 20–40 km in diameter and of about 5–7 km at depths horizontally. With further deepening at a depth of 10–12 km, it splits into two branches whose resistivity increases, approaching background values in the upper mantle. In this case, the lower arm is shifted southward to the area of Sovetskaya Gavan. Thus, this conducting heterogeneity is located from the area in the north of the Datta Village along the coast to the area in the south of Sovetskaya Gavan. The high-resistivity area separating the arms and being visible in Fig. 4*d*, expands with increasing depth and spreads to the east toward the island. It should be noted that conducting inhomogeneities here are also manifested in the uppermost layers at depths of 0–200 m, reflecting surface local conducting formations, mainly represented by the complex configuration of shallow water and sediments within them. Then they are absent down to a depth of 2 km. With further deepening, a conductive heterogeneity stands out in contrast to the bottom of the Earth's crust. High resistivity

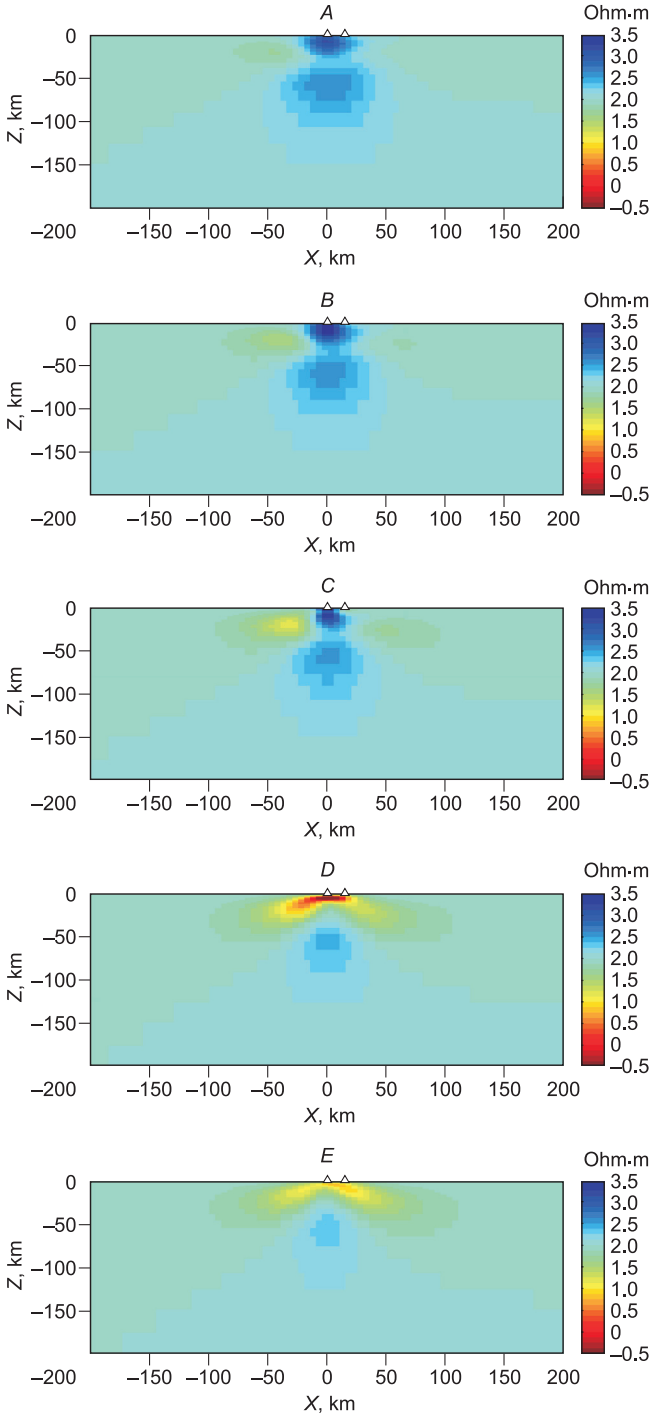

Fig. 5. Sections of the resistivity of the resulting model in the vicinity of the DTA point in the *XZ* planes in vertical layers 5 km thick at the distances of their boundaries from the observation point along the *Y* axis by –90 ... –85 km (*A*), –80… –75 km (*B*), –70… –65 km (*C*), –55… –50 km (*D*), –45… –40 km (*E*). The coordinate system is shown in Fig. 1. View from the positive direction of the Y-axis (from the east). The triangle at the origin indicates the location of the DTA point at $x = 0$, $y = –65$ km in the model coordinate system. The color scale of the resistivity in a logarithmic scale is shown to the right of the figures.

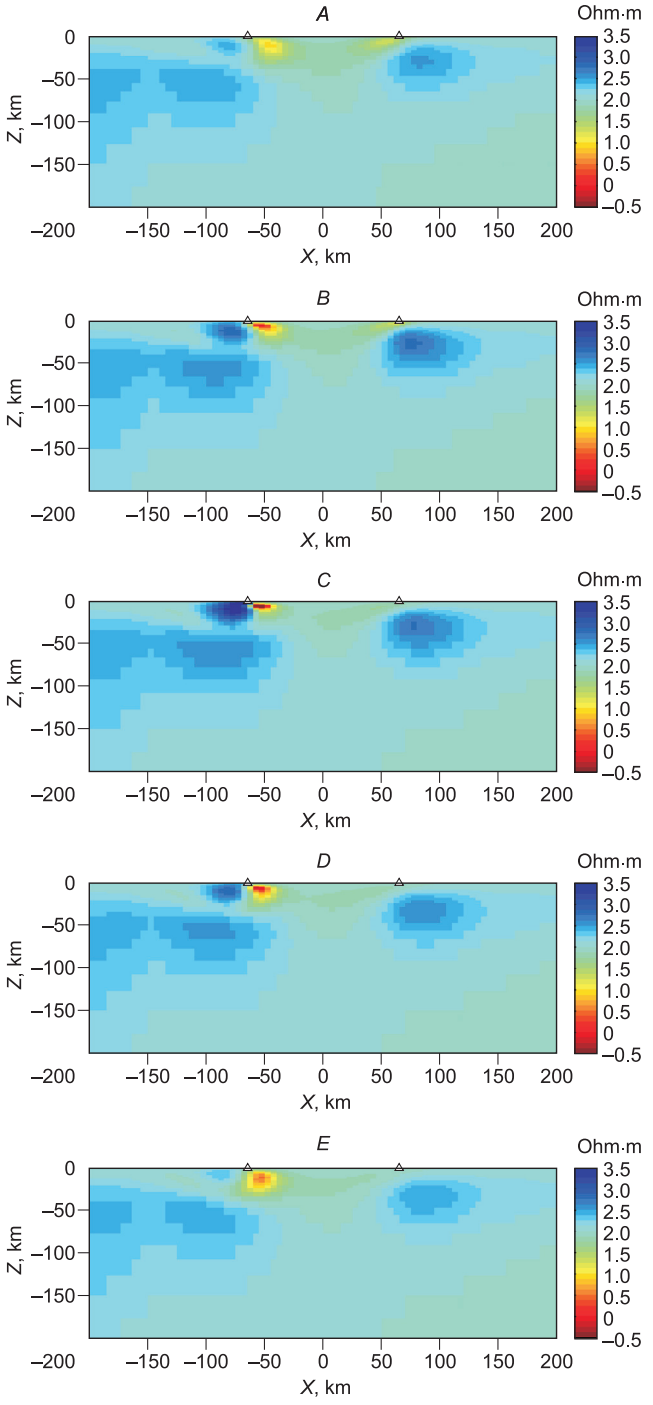

Fig. 6. Vertical sections across the Tatar Strait in the *YZ* plane in vertical layers 5 km thick at the distances of their boundaries from the DTA point along the *X* axis by 25–20 km (*A*), 15–10 km (*B*), 0 ... –5 km (*C*), –10… –15 km (*D*), –20… –25 km (*E*). View from the negative direction of the *X*-axis (from the south). The origin is in the middle of the strait. On the left is DTA, on the right is LSG. The color scale of the resistivity in a logarithmic scale is shown to the right of the figures.

values exceeding 1000 Ohm·m can be seen from the side of the continent, at this point in the section model, and they are the reason for the large values of the tippers.

A similar situation is observed in the vicinity of point LSG with an exception for the fact that the contrast of resistivity anomalies here is much lower and they are not parallel to the coastline in the strait as at point DTA. Here the local conducting inhomogeneity is located in the coastal part of the strait to the northwest of the point, partly spreading into the island territory. As the depth increases, the resistivity of its central part decreases, reaching a minimum of 15 Ohm·m at a depth of 8–12 km, and approaches the resistivity of the starting model in the lower crust.

The meridional longitudinal sections near point DTA are shown in Fig. 5. Here, in the figures, the distances of the profiles from the point along the y axis is expressed in the coordinate system shown in Fig. 1. Their displacement relative to point DTA is estimated by recalculating their values to the system associated with this point, while the y_{DTA} coordinate is determined as follows: $y_{DTA} = y - y_0$ where y_0 is the point coordinate in the original system (y_0 = –65 km) and y denotes the coordinates indicated the figure caption (with account for the sign). Now negative values set directions from a point near the coastline inland and positive values to the Sakhalin Island. Looking at the sections shown in Fig. 5*a* and 5*b* represent 5-km thick vertical layers, starting from distances of –25 ... –20 km from the coastline in sections down to depths of 100–150 km, one can see high-resistivity values in the vicinity of the point and low-resistivity values on the right and left (north and south, respectively) from it. These areas are underlain by a layer with a resistivity of 100 Ohm·m, specified in the starting model. When crossing the coastline in the coastal region of the strait (see Fig. 5*D*, *E*), the left and right low-resistance regions merge, and a pronounced conducting inhomogeneity appears. It is located vertically in the depth range of 2–22 km, and horizontally extends along the coast in the central part for about 100 km, manifesting itself at a distance of more than 30 km from the coast.

Latitudinal sections across the Tatar Strait from north to south through the latitude of point DTA point at selected distances from it are shown in Fig. 6*a–d*. On all sections, with resistivity values exceeding 100 Ohm·m, a conducting region is distinguished under the bottom of the Tatar Strait. In the central part of the strait, it begins at a depth of ≈10 km, continues to ≈50 km and, narrows down, and merges with the background at a depth of about 90 km. It is peculiar how this area is joined with the mainland and the island. Near the mainland, in the coastal part, it sinks sharply to depths of 20–25 km, which may be caused by a fault, but, closer to the island, the conducting strata slowly rises and enters its limits. This behavior of the conducting strata is typical for the sections north of point DTA (see Fig. 6*a*, *b*). Starting from the latitude of point DTA and further to the south, there is spatial differentiation of the resistivity of the stratum in the section under the Tatar Strait. At the most distant profile, it is smoothly joined with the continent with a branch, which gradually rises upward in the lower part with distance from the strait. In the lower right part of all sections, starting from a depth of about 90 km, there is a conductive region plunging at an angle of ≈30° in a direction toward the continent.

RESULTS AND DISCUSSION

First of all, it is important to note that conducting geoelectric inhomogeneities in model sections are given within the framework of the Earth's crust and partly in the upper lithospheric mantle. They are located in the Tatar Strait between observation points, partly penetrating under the island and into the mainland. They are located near the points and can be observed starting at depths of nearly 2 km, and, as the depth increases, they expand and merge together at a depth of about 10–12 km. At the same time, their resistivity reaches minimum values (maximum electric conductivity range) in the central parts at a depth of 5–7 km near point DTA and at 8–12 km at LSG, at which their resistivity (≈15 Ohm·m) is larger as compared to the first point (≈0.5 Ohm·m) as seen from Fig. 4.

The cause for resistivity anomalies at point LSG is determined using seismological data. On the website http://www.ds.iris.edu/seismon/, we use the IRIS earthquake browser and obtain a sample of earthquake hypocenters with a value M = 4–6 near this point from 1973 to 2014. It turns out that, of the 52 crustal earthquakes obtained, 45 have a hypocenter depth of 10 km. The perpendicular projections of the epicenters of these earthquakes onto the surface of the horizontal section of the model at a depth of 10.3 km are shown in Fig. 4*b*. The figure shows that earthquakes are located in an electrical conductivity anomaly region in this depth interval. It should be noted that there is a wider region of crustal earthquakes to the south, within the western edge of the island and the eastern side of the strait (Lomtev et al., 2007), localized along the West Sakhalin Fault. The hypocenters of these crustal earthquakes are also located at depths of about 10 km. Taking this into account, here it is necessary to assume significant fracturing. If it is saturated with fluids released during metamorphism or rising from the lower horizons of the Earth's crust and the upper mantle, conditions for the existence of conductive zones are created.

Usually, electrical conductivity anomalies in the Earth's crust and upper mantle are explained using several mechanisms of its increase. Among them are the presence of water and its solutions in the pores of the rock (Nesbitt, 1993), the graphitization of intergranular and pore space of rocks (Jodicke, 1992; Zhamaletdinov, 1996; Jodicke et al., 2004), their partial melting (Ni et al., 2011), and rock decompaction by local earthquakes with the formation of flooded fracturing (Unsworth et al., 1999; Kissin, 2004). On the other hand, if mantle diapir penetrates into the Earth's crust and its components crystallize, liquid and gaseous fluids begins to evolve during cooling, which, penetrating into the upper ho-

rizons, ensures the unloading of elastic tectonic stresses present therein, i.e., cause earthquakes (Miller, 2013). Rock decompaction near point LSG is also indicated by a chain of gravitational minima. It stretches here in the strait parallel to the coast and at a distance of about 15–20 km from it as can be seen on a WGM map (International Bureau of Gravity) of Bouguer gravity anomalies (WGM2012).

The presence of coal deposits of the Uglegorsk coal-bearing region in the region under study (Zhizhin, 1974) suggests the accumulation of biogenic material here in past epochs, from which graphite can form if it happens to be in a high-temperature zone during metamorphism (Jodicke, 1992). In order for the increased conductivity to be associated with graphitization, it is necessary to assume that the graphite fibers are interconnected, representing a single conductor of electric current at large distances. The existence of such a conductor in this case is hindered by the seismicity of the region, which, during fracturing, disrupts the connectivity of graphite fibers if they are present in the rock. However, the introduction of conducting fluids in this case restores electrical connection between graphite fibers. The possibility of abiogenic formation of graphite in microcracks in the bottom of the Earth's crust by ascending flows of gaseous fluids discharging in the fault zone cannot be ruled out. Taking into account that the heat flux near this point is 60 mW/m^2 (Veselov, 2006), it can be estimated from thermometry that, in regions of recent activation at depths of 10–12 km, the temperature is about 400–500 °C (Cermak and Lastovickova, 1987), which is not enough for the melting of rocks, in which case their electrical conductivity increases. This temperature range allows for the existence of graphite conductivity along grain boundaries, which vanishes at temperatures of about 1000 °C (Yoshino and Noritake, 2011). Therefore, the source of the conductive anomaly should apparently considered to be fluidization and decompaction of the section in this region.

At point DTA, the central area of the local contrast anomaly is located even closer to the surface. The conducting anomaly itself stretches along the coast, plunging to the north and south. In contrast to the opposite shore of the Tatar Strait, there is no noticeable seismic activity, but, in the strait near the continent, there is a positive anomaly region in the gravity field (WGM2012), which matches the anomalous electrical conductivity zone. According to seismic data, a mantle ledge is distinguished here, near which the thickness of the Earth's crust is reduced to 20 km (Khanchuk, 2004). Perhaps, the anomaly is related to its existence. It should be noted that similar near-surface anomalies with high electrical conductivity are identified according to MT and MV methods in rifting regions and in modern volcanism regions (Matsushima et al., 2001; Hill et al., 2009; Bertrand et al., 2012; McGary et al., 2014; Comeau at al., 2015). In these regions, the existence of magma chambers in the upper part of the Earth's crust, containing a large percentage of melts, is assumed. The results are interpreted using the data of laboratory studies pertaining to the electrical conductivity of igneous rocks during melting under various *P–T* conditions typical for the depth intervals studied. In this case, a decrease in the melting point of the rock in the presence of water is observed. Thus, in (Laumonier et al., 2015), by varying the percentage of water in dacite melts, at pressures attained at the depths under study, melting points of about 800 °C are obtained. In this case, the resistivity of melts of about 1 Ohm·m are close to the values determined from the MT sounding data at depths of 5–20 km in these regions. Low resistivity values of 0.1–1.0 Ohm·m, close to the values of the local anomaly at point DTA, are also obtained in experiments on measuring the electrical conductivity of tholeiitic basalt and andesite melts from the Hawaiian Islands (Tyburczy and Waff, 1983) at temperatures of 1200–1400 °C and pressures of 0–1 GPa existing within the Earth's crust.

These results are acceptable for areas of recent volcanic activity, which is not typical for the region under study. There are no heat flux measurements here, which could somewhat clarify the situation. The existence of a thermal spring approximately 30 km from the coast (Poturay et al., 2018) with a water temperature of 50 °C indicates possible temperature activation of the subsoil. It remains to assume that the upper part of the Earth's crust is processed by liquid and gaseous fluids rising along the East Sikhote-Alin deep fault from the mantle ledge. The reality of the existence of the latter in the geological setting of the region is also confirmed by geophysical studies in other similar regions. Thus, on the Atlantic coast of northwestern Namibia in the region of the Cretaceous basalt plateaus in the area of interaction of the plume with the continent, a mantle bulge is recorded in seismic studies (a region of high seismic velocities v_P = 8 km/s in the middle and lower crust) within the same depth interval (Ryberg et al., 2015). From the ledge, a slowly ascending supply channel is traced, and it is assumed that that basaltic magma is poured onto the surface of the continent through it. Figure 6*d, e* represents the cross section of the Tatar Strait to the left of the coastline and shows low-resistivity region slowly ascending to the continent, extending at a distance of about 60–70 km from the coast, and starting from the upper mantle depths under the strait. It is not excluded that this region could have been a supply channel for basaltic eruptions on the continent.

It can be seen on the cross sections in Fig. 6 that the lower crust and the upper mantle to a depth of ≈100 km under the strait have a resistivity of 30–60 Ohm·m. Below, there is a layer with a resistance of 100 Ohm·m, with a conducting wedge with a lower resistance being plunged under it on the right. The resistivities of these conductive layers correspond to those of basaltic melts for *P–T* conditions at these depths (Dai et al., 2015). To the north and south of point DTA, the upper conductive zone connects to a plunging wedge region, denoting a branch from the deep conductor into the Tatar Strait region.

CONCLUSION

The performed MV sounding of the Tatar Strait and the 3D inversion of their results make it possible to construct a geoelectric model of the deep structure of the strait to the upper mantle depths. The model shows two local highly conductive anomalies near the continent and the island at depths of 5–7 and 8–12 km, respectively. Their location at the top of the Earth's crust in the region of development of faults and mantle ledges near the continent suggests that they are caused by these features of the geological structure of the region. The studies carried out have established that, near the continent, the anomaly is elongated along the coast of the strait, and, near the island, it has an isometric shape in the horizontal plane. The interesting fact that the island anomaly matches the zones of local crustal earthquakes requires further research.

Throughout the entire length of the Tatar Strait in the modeling area, from depths of the first kilometers to the upper mantle depths, its geoelectric section has a higher electrical conductivity than adjacent areas. The model shows a conductive block descending under the Tatar Strait from the Sea of Okhotsk. At depths of more than 100 km, it can be related to a plunging slab (Martynov and Khanchuk, 2013).

In conclusion, it should be noted that the use of 3D inversion of MV data at the two points makes it possible to estimate the main features and localization of geoelectric inhomogeneities in the Tatar Strait section. The use of profile and areal observations in the region for 3D inversion undoubtedly increases the detail of its deep structure, considering that the program allows inverting 100 or more observation points (Egbert et al., 2017). Undoubtedly, point, profile, and areal recording of electrical and magnetic variations on ice or at the bottom of the Tatar Strait radically improve the illumination of the geoelectric section of its underwater part. Efforts are directed at their implementation up to the development or acquisition of sea bottom stations.

The authors are grateful to Dr. G. Egbert for providing the ModEM program and the possibility of using it, to Dr. A. Kelbert for consultations during the launch of the program, and to the creators of all the websites cited in the article for access to the data presented on them.

The study was carried out with the financial support of the state task on issue No. 0271-2019-0002, registration number AAAA-A17-117030110032-3, and Grant No. 18-1-004 of the program "Far East" of the Far Eastern Branch of the Russian Academy of Sciences.

REFERENCES

Berdichevsky, M.N., Dmitriev, V.I., 2008. Models and Methods of Magnetotellurics. Springer-Verlag Berlin Heidelberg, doi: 10.1007/978-3-540-77814-1_1.

Bertrand, E.A., Caldwell, T.G., Hill, G.J., Wallin, E.L., Bennie, S.L., Cozens, N., Wameyo, P., 2012. Magnetotelluric imaging of upper crustal convection plumes beneath the Taupo Volcanic Zone, New Zealand. Geophys. Res. Lett. 39 (2), Article L02304, doi: 10.1029/2011GL050177.

Campanya, J., Ogaya, X., Jones, A.G., Rath, V., Vozar, J., Meqbel, N., 2016. The advantages of complementing MT profiles in 3-D environments with geomagnetic transfer function and interstation horizontal magnetic transfer function data: results from a synthetic case study. Geophys. J. Int. 207, 1818–1836, doi: 10.1093/gji/ggw357.

Cermak, V., Lastovickova, M., 1987. Temperature profiles in the Earth of importance to deep electrical conductivity models. Pure Appl. Geophys. 125 (2–3), 255–284.

Comeau, M.J., Unsworth, M.J., Ticona, F., Sunagua, M., 2015. Magnetotelluric images of magma distribution beneath Volcán Uturuncu, Bolivia: Implications for magma dynamics. Geology 43 (3), 243–246, doi: 10.1130/G36258.1.

Dai, L., Jiang, J., Li, H., Hu, H., Hui, K., 2015. Electrical conductivity of hydrous natural basalts at high temperatures and pressures. J. Appl. Geophys. 112, 290–297.

Egbert, G.D., Kelbert, A., 2012. Computational recipes for electromagnetics inverse problems. Geophys. J. Int. 189, 251–267, doi: 10.1111/j.1365-246X.2011.05347.x.

Egbert, G.D., Meqbel, N., Kelbert, A., 2017. Some results from ModEM3DMT, the freely available OSU 3D MT inversion code, in: 6th International Symposium on Three-Dimensional Electromagnetics. Berkeley, California, https://kmstechnologies.com/Files/Flyer%20for%20website/Gary_Egbert_ModEM.pdf.

Esin, S.V., Kutolin, V.A., Prusevich, A.A., 1990. Volcanism in the Middle Part of Eastern Sikhote-Alin (a Datta Cape – Syurkum Cape area) [in Russian]. IGiG SO AN SSSR, Novosibirsk.

Esin, S.V., Prusevich, A.A., Kutolin, V.A., 1992. Late Cenozoic Volcanism and the Deep Structure of Eastern Sikhote-Alin [in Russian]. Nauka, Novosibirsk.

Hill, G.J., Caldwell, T.G., Heise, W., Chertkoff, D.G., Bibby, H.M., Burgess, M.K., Cull, J.P., Cas, R.A., 2009. Distribution of melt beneath Mount St Helens and Mount Adams inferred from magnetotelluric data. Nat. Geosci. 2 (11), 785–789, doi: 10.1038/ngeo661.

Jodicke, H., 1992. Water and graphite in the Earth's crust – An approach to interpretation of conductive models. Surv. Geophys. 13 (4), 381–407, doi: 10.1007/BF01903484.

Jodicke, H., Kruhl, J., Ballhaus, C., Giese, P., Untied, J., 2004. Syngenetic, thin graphite-rich horizons in lower crustal rocks from the Serre San Bruno, Calabria (Italy), and implications for the nature of high-conducting deep crustal layers. Phys. Earth Planet. Int. 141, 37–58.

Kelbert, A., Meqbel, N.M., Egbert, G.D., Tandon, K., 2014. ModEM: A modular system for inversion of electromagnetic geophysical data. Comp. Geosci. 66, 40–53, doi: 10.1016/j.cageo.2014.01.010

Khanchuk, A.I. (Ed.), 2004. Geology, Geodynamics, and Oil and Gas potential of Sedimentary Basins of the Tatar Strait, in: Sedimentary basins of the Russian East, Issue 2 [in Russian]. Vladivostok, Izd. DVO RAN.

Kissin, I.G., 2004. Main types of fluid systems in the consolidated crust and their relationship with tectonic structures. Dokl. Earth Sci. 395 (3), 319–323.

Kuhn, C., Kuster, J., Brasse, H., 2014. Three-Dimensional Inversion of Magnetotelluric Data from the Central Andean Continental Margin. Earth Planets Space, 66, Article 112, doi: 10.1186/1880-5981-66-112.

Laumonier, M., Gaillard, F., Sifre, D., 2015. The effect of pressure and water concentration on the electrical conductivity of dacitic melts: Implication for magnetotelluric imaging in subduction areas. Chem. Geol., 418, 66–76, doi: 10.1016/j.chemgeo.2014.09.019.

Lomtev, V.L., Nikiforov, S.P., Kim, C.U., 2007. Tectonic aspects of the crustal seismicity of Sakhalin. Vestnik DVO RAN, No. 4, 64–71.

Lyubimova, E.A., Nikitina, V.N., Tomara, G.A., 1976. Thermal Fields of Internal and Marginal Seas of the USSR [in Russian]. Nauka, Moscow.

Martynov, Yu.A., Khanchuk, A.I., 2013. Cenozoic volcanism of the Eastern Sikhote Alin: petrological studies and outlooks. Petrology 21 (1), 85–99.

Matsushima, N., Oshima, H., Ogawa, Y., Takakura, S., Satoh, H., Utsugi, M., Nishida, Y., 2001. Magma prospecting in Usu volcano, Hokkaido, Japan, using magnetotelluric soundings. J. Volcanol. Geotherm. Res., 109 (4), 263–277, doi: 10.1016/S0377-0273(00)00320-6.

McGary, R.S., Evans, R.L., Wannamaker, P.E., Elsenbeck, J., Rondenay, S., 2014. Pathway from subducting slab to surface for melt and fluids beneath Mount Rainier. Nature 511 (7509), 338–340, doi: 10.1038/nature13493.

Miller, S., 2013. The Role of fluids in tectonic and earthquake processes, in: Dmowska, R. (Ed.), Advances in Geophysics. Elsevier, Amsterdam, Vol. 54, pp. 1–38.

Nesbitt, B., 1993. Electrical resistivities of crustal fluids. J. Geophys. Res 98 (B3), 4301–4310.

Ni, H., Keppler, H., Behrens, H., 2011. Electrical conductivity of hydrous basaltic melts: implications for partial melting in the upper mantle. Contrib. Mineral. Petrol. 162, 637–650, doi: 10.1007/s00410-011-0617-4.

Patro, P.K., Egbert, G.D., 2008. Regional conductivity structure of Cascadia: Preliminary results from 3D inversion of USArray transportable array magnetotelluric data. Geophys. Res. Lett. 35, L20311, doi: 10.1029/2008GL035326.

Patro, P.K., Egbert, G.D., 2011. Application of 3D inversion to magnetotelluric profile data from the Deccan Volcanic Province of Western India. Phys. Earth Planet. Int. 187, 33–46, doi: 10.1016/j.pepi.2011.04.005.

Poturay, V.A., Strochinskaya, S.S., Kompanichenko, V.N., 2018. Complex biochemical characteristics of the Tumnin spring thermal waters. Regional'nye Problemy 21 (1), 22–30.

Ryberg, T., Haberland, C., Haberlau, T., Weber, M.H., Bauer, K., Behrmann, J.H., Jokat, W. 2015. Crustal structure of northwest Namibia: Evidence for plume-rift-continent interaction. Geology 43 (8), 739–742, doi: 10.1130/G36768.1.

Samrock, F., Kuvshinov, A., Bakker, J., Jacson, A., Fisseha, S., 2015. 3-D analysis and interpretation of magnetotelluric data from the Aluto-Langano geothermal field, Ephiopia. Geophys. J. Int. 202 (3), 1923–1948, doi: 10.1093/gji/ggv270.

Tietze, K., Ritter, O., 2013. Three-dimensional magnetotelluric inversion in practice-the electrical conductivity structure of the San Andreas Fault in Central California. Geophys. J. Int. 195 (1), 130–197, doi: 10.1093/gji/ggt234.

Tietze, K., Ritter, O., Egbert, G.D., 2015. 3-D inversion of the magnetotelluric phase tensor and vertical magnetic transfer function. Geophys. J. Int. 203 (2), 1128–1148, doi: 10.1093/gji/ggv347.

Tronov, Yu.A., Kharakhinov, V.V., Kononov, V.E., Pudikov, E.G., 1987. The North-Tatar oil and gas bearing basin. Tikhookeanskaya geologiya, No. 6, 45–49.

Tyburczy, J.A., Waff, H.S., 1983. Electrical conductivity of molten basalt and andesite to 25 kbar pressure: geophysical significance and implications for charge transport and melt structure. J. Geophys. Res. 88, 2413–2430.

Unsworth, M., Egbert, G., Booker, J., 1999. High-resolution electromagnetic imaging of the San Andreas Fault in Central California. J. Geophys. Res. 104, 1131–1150, doi: 10.1029/98JB01755.

Varnavskii, V.G., 1994. Prospects for oil-and-gas presence on the circumcontinental shelf, Tatar Strait. Tikhookeanskaya Geologiya, No. 3, 33–44.

Veselov, O.V., 2006. Geometric studies, in: Sergeev, K.F. (Ed.), Tectonic Zoning and Hydrocarbon Potential of the Sea of Okhotsk [in Russian]. Nauka, Moscow.

Volgin, P.F., Kochergin, E.V., 2006. Anomalously magnetic field, in: Sergeev, K.F. (Ed.), Tectonic Zoning and Hydrocarbon Potential of the Sea of Okhotsk [in Russian]. Nauka, Moscow.

Volgin, P.F., Senachin, V.N., 2006. Anomalously gravitational field, in: Sergeev, K.F. (Ed.), Tectonic Zoning and Hydrocarbon Potential of the Sea of Okhotsk [in Russian]. Nauka, Moscow.

Yoshino, T., Noritake, F., 2011. Unstable graphite films on grain boundaries in crustal rocks. Earth Planet. Sci. Lett. 306 (3), 186–192.

Zhamaletdinov, A.A., 1996. Graphite in the Earth's Crust and electrical conductivity anomalies. Izvestiya, Physics of the Solid Earth 32 (4), 272–288.

Zhizhin, D.P., 1996. Coal, in: Sidorenko, A.V. (Ed.), USSR Geology, the Sakhalin Island, and and Minerals (in Russian). Nedra, Moscow, Issue 33, pp. 13–57.

Editorial responsibility: I.N. Yeltsov